Acta Polytechnica CTU Proceedings **54**:34–40, 2025
https://doi.org/10.14311/APP.2025.54.0034

Published by the Czech Technical University in Prague

OPTIMISING TRUSS-BASED METAMATERIALS FOR UNIMODAL AND PENTAMODAL BEHAVIOUR

Nataša Jošková*, Marek Tyburec, Martin Doškář

Czech Technical University in Prague, Faculty of Civil Engineering, Department of Mechanics, Thákurova 7, 166 29 Prague 6, Czech Republic

* corresponding author: joskonat@cvut.cz

Abstract. Our study focuses on the optimisation of the internal structure of unimodal and pentamodal metamaterials, modelled as three-dimensional linear elastic lattice structures. For optimisation, we represent the metamaterials with discrete truss models of their respective Periodic Unit Cells (PUCs), whose effective response is determined by the first-order numerical homogenisation. The optimisation is formulated as an inverse homogenisation problem with objective functions comprising a ratio of selected eigenvalues of the effective stiffness matrix, which allows us to dispense with the traditional volume constraint and solve the optimisation problem with a simple gradient method combined with the line search method. We demonstrate the efficacy of the formulation with a design of a unimodal material compliant in a chosen shear deformation mode and we also show that our formulation recovers the traditional pentamodal metafluid.

Keywords: Optimisation, unimodal metamaterial, pentamodal metamaterial, first-order homogenisation, Periodic Unit Cell.

1. Introduction

Metamaterials have physical properties that surpass those commonly found in nature. Moreover, these unique properties arise primarily from the microstructure of metamaterials rather than the chemical or physical characteristics of their bulk constituents [1]. In our study, we focus on three-dimensional unimodal and pentamodal mechanical metamaterials [2]. The modality of these materials is derived from the number of free modes of deformation [3], i.e., homogeneous deformations that do not result in an increase in the stored strain energy. In particular, a unimodal metamaterial is pliable in one specific direction but very stiff in the other modes of deformation. Conversely, pentamodal metamaterials behave like a fluid (sometimes pentamodal metamaterials are called metafluids), i.e., while they are almost incompressible, they can be easily deformed in a deviatoric way.

Because of their unique properties, these metamaterials can be applied in various advanced fields. One of the most extensively researched applications is their ability to create acoustic band gaps – specific frequency ranges in which sound waves are unable to propagate through the material due to disrupted transmission [4, 5]. This behaviour makes them highly effective for applications in noise control, vibration isolation, and acoustic filtering, even underwater [6]. Another potential application is for cloaking devices that transform waves to make objects invisible or undetectable by bending light or sound, effectively preventing detection or visual observation [7]. The ability to control the propagation of elastic waves also makes them highly effective for seismic isolation [8, 9].

Multimodal metamaterials have garnered significant research interest, with pentamodal metamaterials being a primary focus. However, much of the research involves modifying the original pentamodal structure introduced by Milton and Cherkaev [3] to enhance its overall performance. This includes investigating different shapes [11] and sizes [12] of cross-sectional areas, adding spherical masses to the nodes [13] and incorporating stiffening plates between the metamaterial layers [14], even with different microstructures [10]. In addition, researchers managed both to introduce anisotropy by shifting the central part of the microstructure [15, 16], and, conversely, employ symmetrical designs [17].

In contrast, optimising metamaterial topology through inverse homogenisation, pioneered by the seminal work of Sigmund [18], often revolves around enhancing the bulk or shear modulus [19], tailoring Poisson's ratio [20], and designing materials that are both lightweight and stiff [21] or that follow a predefined macroscopic response in the case of nonlinear models [22]. Relatively few studies have focused on optimising multimodal metamaterial microstructures. In addition to inverse homogenisation, genetic algorithms have been used to optimise the ratio of eigenfrequencies [23] and components of the homogenised stiffness matrix [24], or to maximise bandwidth [25] to improve the acoustic band gap.

In this work, we use the inverse homogenisation with the objective function based on the ratio of effective stiffness's eigenvalues (or its analogues), distinct from previously discussed approaches. Our approach allows for the optimisation of specific deformation modes and enables the analytical expression of the objective function's gradient. In addition, it naturally avoids

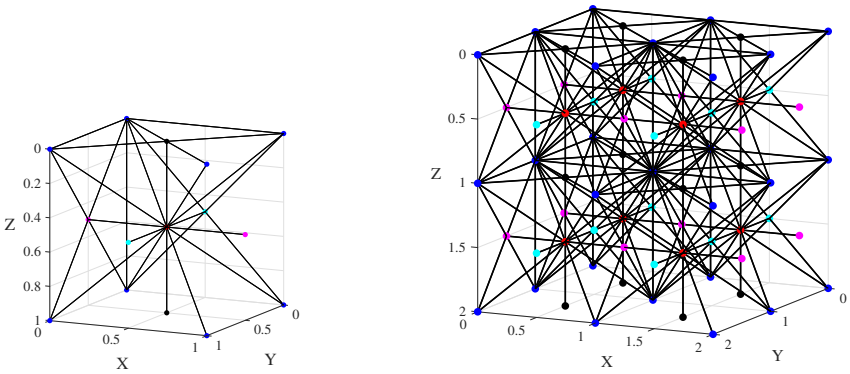

FIGURE 1. Two periodic ground structures considered in the study: smaller ground structure with dimensions of $1 \times 1 \times 1$ (left) and larger ground structure with dimensions of $2 \times 2 \times 2$ (right).

the need for the volume constraint.

To keep this contribution self-contained, the Methodology section briefly covers also the essentials of the first-order homogenisation (Section 2.1) in addition to the objective formulation and the adopted optimisation strategy (Section 2.3). We demonstrate the efficacy of the proposed objective formulation with two examples (one for the unimodal and one for pentamodal metamaterial) in Section 3 and summarise our findings in Section 4.

2. METHODOLOGY

2.1. NUMERICAL MODEL

Assuming the metamaterial as a three-dimensional periodic truss structure allowed us to investigate the response of a Periodic Unit Cell (PUC) as its Representative Volume Element. We modelled the PUC with a ground structure containing discrete 3D trusses with predefined positions and orientations as shown in Figure 1. As the shape of cross sections does not affect the stiffness of the truss structure, for this study, we additionally assumed circular cross sections with area a_i for each truss rod i as the primal unknowns for optimisation, collectively stored in a vector of cross-sectional areas a.

To determine the mechanical response of the PUC, we used a linear truss model, governed by the global stiffness matrix $\mathsf{K}(\mathsf{a})$ assembled from the local contributions of individual rods such that formally

$$\mathsf{K}(\mathsf{a}) = \sum_i \mathsf{L}_i^\mathsf{T} \mathsf{T}_i^\mathsf{T} \mathsf{K}_i^\ell(a_i) \mathsf{T}_i \mathsf{L}_i \,, \tag{1}$$

where L_i denotes Boolean localisation matrices, T_i is a transformation matrix containing directional cosines of the i-th rod, and the element stiffness matrix K_i^ℓ in the local coordinate system reads as

$$\mathsf{K}_i^\ell(a_i) = \frac{E a_i}{L_i} \begin{bmatrix} 1 & -1 \\ -1 & 1 \end{bmatrix} , \tag{2}$$

where E stands for Young's modulus and L_i refers to the initial length of the i-th rod.

2.2. FIRST-ORDER HOMOGENISATION

The homogenisation determines the effective response of a heterogeneous PUC as if it were an equivalent homogeneous material point subjected to the same uniform strain field E. For the linear problem considered here, the homogenised response is captured by the effective stiffness matrix $\mathsf{D}^{\mathrm{hom}}(\mathsf{a})$.

In our study, we employed the first order numerical homogenisation [26] to obtain the effective properties of the metamaterial. The total displacement field $\vec{u}(\vec{x})$ was thus assumed in the form

$$\vec{u}(\vec{x}) = \vec{u}^{\,\mathbf{E}}(\vec{x}) + \vec{u}^{\,*}(\vec{x}) \,, \tag{3}$$

where $\vec{u}^{\,\mathbf{E}}$ denotes the macroscopic part of the displacement field and $\vec{u}^{\,*}$ is the fluctuation caused by the heterogeneity of the metamaterial [27].

For the discrete system, degrees of freedom (DOFs) related to the macroscopic displacement of the j-th node are coupled to the vectorial representation of the symmetric second-order tensor $\mathbf{E}$ via matrix Q_j containing coordinates of node j,

$$\mathsf{u}_j^\mathsf{E} = \begin{bmatrix} x_j & 0 & 0 & 0 & \frac{1}{2}z_j & \frac{1}{2}y_j \\ 0 & y_j & 0 & \frac{1}{2}z_j & 0 & \frac{1}{2}x_j \\ 0 & 0 & z_j & \frac{1}{2}y_j & \frac{1}{2}x_j & 0 \end{bmatrix} \mathsf{E} = \mathsf{Q}_j \, \mathsf{E} \,. \tag{4}$$

The displacement degrees of freedom u, including both the macroscopic and fluctuation part, then follow as

$$\mathsf{u} = \begin{bmatrix} \mathsf{Q} & \mathsf{I} \end{bmatrix} \begin{bmatrix} \mathsf{E} \\ \mathsf{u}^* \end{bmatrix} = \widehat{\mathsf{Q}} \, \widehat{\mathsf{u}} \,, \tag{5}$$

where Q contains vertically concatenated contributions Q_j, I stands for the identity matrix, and u^* denotes the fluctuation DOFs. Due to the assumed periodic boundary conditions, not all DOFs in u^* are independent. Accounting for the periodic source-image pairs and preventing rigid body motions by setting zero fluctuation at one selected node, the fluctuation DOFs can be expressed in terms of a subset of unknowns v,

$$\widehat{\mathsf{u}} = \begin{bmatrix} \mathsf{E} \\ \mathsf{u}^* \end{bmatrix} = \begin{bmatrix} \mathsf{I} & 0 \\ 0 & \mathsf{P} \end{bmatrix} \begin{bmatrix} \mathsf{E} \\ v \end{bmatrix} = \widehat{\mathsf{P}} \, \widehat{v} \,, \tag{6}$$

with P being a Boolean matrix facilitating the discussed boundary conditions.

Combining the discrete first-order displacement decomposition (5) and periodicity enforcement (6) leads to the strain energy formula of a PUC

$$\begin{aligned}\mathcal{E}(\mathsf{E},v) &= \frac{1}{2}\,\widehat{v}^{\mathsf{T}}\widehat{\mathsf{P}}^{\mathsf{T}}\widehat{\mathsf{Q}}^{\mathsf{T}}\mathsf{K}(\mathsf{a})\,\widehat{\mathsf{Q}}\,\widehat{\mathsf{P}}\,\widehat{v}\\ &= \frac{1}{2}\begin{bmatrix}\mathsf{E}\\ v\end{bmatrix}^{\mathsf{T}}\begin{bmatrix}\mathsf{Q}^{\mathsf{T}}\mathsf{K}(\mathsf{a})\mathsf{Q} & \mathsf{Q}^{\mathsf{T}}\mathsf{K}(\mathsf{a})\mathsf{P}\\ \mathsf{P}^{\mathsf{T}}\mathsf{K}(\mathsf{a})\mathsf{Q} & \mathsf{P}^{\mathsf{T}}\mathsf{K}(\mathsf{a})\mathsf{P}\end{bmatrix}\begin{bmatrix}\mathsf{E}\\ v\end{bmatrix} \qquad (7)\\ &= \frac{1}{2}\begin{bmatrix}\mathsf{E}\\ v\end{bmatrix}^{\mathsf{T}}\begin{bmatrix}\widehat{\mathsf{K}}_{\mathsf{EE}}(\mathsf{a}) & \widehat{\mathsf{K}}_{\mathsf{E}v}(\mathsf{a})\\ \widehat{\mathsf{K}}_{v\mathsf{E}}(\mathsf{a}) & \widehat{\mathsf{K}}_{vv}(\mathsf{a})\end{bmatrix}\begin{bmatrix}\mathsf{E}\\ v\end{bmatrix}.\end{aligned}$$

From the homogenisation perspective, v can be treated as internal unknowns, which can be uniquely solved for a prescribed E, leaving us with the condensed form

$$\begin{aligned}\widetilde{\mathcal{E}}(\mathsf{E}) &= \frac{1}{2}\,\mathsf{E}^{\mathsf{T}}\left(\widehat{\mathsf{K}}_{\mathsf{EE}}(\mathsf{a}) - \widehat{\mathsf{K}}_{\mathsf{E}v}(\mathsf{a})\widehat{\mathsf{K}}_{vv}^{-1}(\mathsf{a})\widehat{\mathsf{K}}_{v\mathsf{E}}(\mathsf{a})\right)\mathsf{E}\\ &= \frac{1}{2}\,\mathsf{E}^{\mathsf{T}}\mathsf{K}^{\mathrm{eff}}(\mathsf{a})\mathsf{E}\,. \qquad (8)\end{aligned}$$

Comparing the last row of (8) with an expression for the strain energy stored in a homogeneous material of volume V subjected to E yields the final formula for the effective stiffness matrix

$$\mathsf{D}^{\mathrm{hom}}(\mathsf{a}) = \frac{1}{V}\mathsf{K}^{\mathrm{eff}}(\mathsf{a})\,. \qquad (9)$$

For a detailed exposition and discussion of the adopted homogenisation scheme, we kindly refer the reader to our previous work [28].

2.3. Topology optimisation

To optimise the structure of multimodal metamaterials, we utilised the inverse homogenisation [18] with an objective function $\mathcal{O}$ comprising a ratio between a projected stiffness α, defined via a unit modal deformation p as

$$\alpha(\mathsf{a}) = \mathsf{p}^{\mathsf{T}}\mathsf{D}^{\mathrm{hom}}(\mathsf{a})\mathsf{p}\,, \qquad (10)$$

and k-th largest eigenvalue λ_k of the residual stiffness matrix $\mathsf{D}^{\mathrm{res}}$ obtained by subtracting the contribution of the projected stiffness α, i.e.

$$\mathsf{D}^{\mathrm{res}}(\mathsf{a}) = \mathsf{D}^{\mathrm{hom}}(\mathsf{a}) - \alpha(\mathsf{a})\mathsf{p}\mathsf{p}^{\mathsf{T}}\,. \qquad (11)$$

In particular, the objective function for a unimodal metamaterial contains the fifth largest eigenvalue (out of six) of $\mathsf{D}^{\mathrm{res}}$, as its goal is to maximise the gap between the compliant mode pertinent to α and the second smallest stiffness eigenvalue (recall that the smallest eigenvalue of $\mathsf{D}^{\mathrm{res}}$ is zero by definition (11)),

$$\mathcal{O}^{\mathrm{I}}(\mathsf{a}) = \frac{\lambda_5(\mathsf{a})}{\alpha^{\mathrm{I}}(\mathsf{a})}\,, \qquad (12)$$

while the objective function for a pentamodal material includes the largest eigenvalue,

$$\mathcal{O}^{\mathrm{V}}(\mathsf{a}) = \frac{\alpha^{\mathrm{V}}(\mathsf{a})}{\lambda_1(\mathsf{a})}\,, \qquad (13)$$

because all other stiffness components shall vanish compared to the stiffness α^{V} in a predefined mode p.

This objective function is volume independent as both α and λ scale linearly with the linear scaling of a, and thus no additional volume constraint is needed. Formally, our optimisation problem reads

$$\max_{\mathsf{a}}\ \mathcal{O}^{\bullet}(\mathsf{a}) \qquad (14a)$$

$$\underline{a} \le a_i \le\ \overline{a}\,, \qquad (14b)$$

where we set the upper bound $\overline{a}$ such that the diameter of the largest circular cross-section is at maximum one tenth of the shortest truss rod in the ground structure, and the lower bound $\underline{a} = 10^{-4}\cdot\overline{a}$ is posed to avoid an ill-conditioned system in homogenisation (8). Note that $\bullet$ stands either for I or for V such that (14) covers both (12) and (13).

Despite a seemingly complex structure of the objective, a gradient with respect to the design variables a is readily available via the chain rule, i.e.

$$\frac{\partial}{\partial a_i}\mathcal{O}^{\mathrm{I}}(\mathsf{a}) = \frac{\frac{\partial\lambda_5(\mathsf{a})}{\partial a_i}\alpha^{\mathrm{I}}(\mathsf{a}) - \frac{\partial\alpha^{\mathrm{I}}(\mathsf{a})}{\partial a_i}\lambda_5(\mathsf{a})}{\alpha^{\mathrm{I}2}(\mathsf{a})} \qquad (15)$$

and

$$\frac{\partial}{\partial a_i}\mathcal{O}^{\mathrm{V}}(\mathsf{a}) = \frac{\frac{\partial\alpha^{\mathrm{V}}(\mathsf{a})}{\partial a_i}\lambda_1(\mathsf{a}) - \frac{\partial\lambda_1(\mathsf{a})}{\partial a_i}\alpha^{\mathrm{V}}(\mathsf{a})}{\lambda_1^2(\mathsf{a})}\,, \qquad (16)$$

respectively.

The sensitivity of the projected stiffness α with a given p follows directly from the definition (10)

$$\frac{\partial\alpha(\mathsf{a})}{\partial a_i} = \mathsf{p}^{\mathsf{T}}\frac{\partial\mathsf{D}^{\mathrm{hom}}(\mathsf{a})}{\partial a_i}\mathsf{p}\,. \qquad (17)$$

A similar expression also holds for the sensitivity of the k-th largest eigenvalue, that is

$$\frac{\partial\lambda_k(\mathsf{a})}{\partial a_i} = \mathsf{v}_k^{\mathsf{T}}\frac{\partial\mathsf{D}^{\mathrm{res}}(\mathsf{a})}{\partial a_i}\mathsf{v}_k\,, \qquad (18)$$

where v_k is the eigenvector pertinent to the k-th largest eigenvalue and

$$\frac{\partial\mathsf{D}^{\mathrm{res}}(\mathsf{a})}{\partial a_i} = \frac{\partial\mathsf{D}^{\mathrm{hom}}(\mathsf{a})}{\partial a_i} - \frac{\partial\alpha(\mathsf{a})}{\partial a_i}\,\mathsf{p}\,\mathsf{p}^{\mathsf{T}}\,. \qquad (19)$$

The last missing link in the chain rule is the sensitivity of the effective stiffness matrix

$$\begin{aligned}&\frac{\partial\mathsf{D}^{\mathrm{hom}}(\mathsf{a})}{\partial a_i} = \frac{1}{V}\frac{\partial\mathsf{K}^{\mathrm{eff}}(\mathsf{a})}{\partial a_i}\\ &= \frac{1}{V}\frac{\partial}{\partial a_i}\left(\widehat{\mathsf{K}}_{\mathsf{EE}}(\mathsf{a}) - \widehat{\mathsf{K}}_{\mathsf{E}v}(\mathsf{a})\left[\widehat{\mathsf{K}}_{vv}(\mathsf{a})\right]^{-1}\widehat{\mathsf{K}}_{v\mathsf{E}}(\mathsf{a})\right).\end{aligned} \qquad (20)$$

Dropping the explicit dependence on a and using the terse notation $\widehat{\mathsf{K}}_{\bullet\bullet,a_i}$ for the partial derivative with respect to a_i, we obtain

$$\begin{aligned}\frac{\partial\mathsf{K}^{\mathrm{eff}}}{\partial a_i} &= \widehat{\mathsf{K}}_{\mathsf{EE},a_i} - \widehat{\mathsf{K}}_{\mathsf{E}v,a_i}\widehat{\mathsf{K}}_{vv}^{-1}\widehat{\mathsf{K}}_{v\mathsf{E}}\\ &\quad + \widehat{\mathsf{K}}_{\mathsf{E}v}\widehat{\mathsf{K}}_{vv}^{-1}\widehat{\mathsf{K}}_{vv,a_i}\widehat{\mathsf{K}}_{vv}^{-1}\widehat{\mathsf{K}}_{v\mathsf{E}} - \widehat{\mathsf{K}}_{\mathsf{E}v}\widehat{\mathsf{K}}_{vv}^{-1}\widehat{\mathsf{K}}_{v\mathsf{E},a_i}\\ &= \widehat{\mathsf{K}}_{\mathsf{EE},a_i} - \widehat{\mathsf{K}}_{\mathsf{E}v,a_i}\Theta + \Theta^{\mathsf{T}}\widehat{\mathsf{K}}_{vv,a_i}\Theta - \Theta^{\mathsf{T}}\widehat{\mathsf{K}}_{v\mathsf{E},a_i}\,, \qquad (21)\end{aligned}$$

where Θ is the solution to an adjoin problem

$$\widehat{\mathsf{K}}_{vv}\Theta = \widehat{\mathsf{K}}_{v\mathsf{E}}\,. \tag{22}$$

The sensitivities of the four sub-blocks $\widehat{\mathsf{K}}_{\mathsf{EE}}$, $\widehat{\mathsf{K}}_{\mathsf{E}v}$, $\widehat{\mathsf{K}}_{v\mathsf{E}}$, and $\widehat{\mathsf{K}}_{vv}$ follow the same pattern as they are (potentially asymmetric) projections of $\mathsf{K}(\mathsf{a})$, recall (7), and thus they all require only

$$\frac{\partial \mathsf{K}(\mathsf{a})}{\partial a_i} = \mathsf{L}_i^{\mathsf{T}}\mathsf{T}_i^{\mathsf{T}}\frac{E}{L_i}\begin{bmatrix}1 & -1\\ -1 & 1\end{bmatrix}\mathsf{T}_i\mathsf{L}_i\,. \tag{23}$$

Being able to express the gradient of the objective function analytically led us to the adoption of a steepest ascent method. To compensate for the fact that we did not compute a Hessian, we supplemented the steepest ascent method with the line search method equipped with the Armijo rule [29].

We started by randomly initialising feasible design variables a that satisfy the box constraints (14). In each iteration, we first calculated the gradient of the objective function $\nabla\mathcal{O}$ using the expressions introduced above. Next, we defined a modified gradient $\widehat{\nabla\mathcal{O}}(\mathsf{a})$ by projecting the original one on the active box constraints such that

$$\widehat{\nabla\mathcal{O}}_i(\mathsf{a}) = \begin{cases} 0 & \text{if } \mathsf{a}_i = \overline{a} \ \wedge\ \nabla\mathcal{O}_i(\mathsf{a}) > 0\\ 0 & \text{if } \mathsf{a}_i = \underline{a} \ \wedge\ \nabla\mathcal{O}_i(\mathsf{a}) < 0\\ \nabla\mathcal{O}_i(\mathsf{a}) & \text{otherwise.}\end{cases} \tag{24}$$

The modified gradient then constituted the search direction for the inexact one-dimensional maximisation in the current iteration. Starting with an initial step length computed as the minimum of candidate lengths $\widetilde{\nu}_i$ ensuring that the box constraints are not violated in the new state, i.e.,

$$\widetilde{\nu}_i = \begin{cases} (\overline{a} - \mathsf{a}_i)/\widehat{\nabla\mathcal{O}_i(\mathsf{a})} & \text{if } \widehat{\nabla\mathcal{O}}_i(\mathsf{a}) > 0\\ (\underline{a} - \mathsf{a}_i)/\widehat{\nabla\mathcal{O}}_i(\mathsf{a}) & \text{if } \widehat{\nabla\mathcal{O}}_i(\mathsf{a}) < 0\\ 0 & \text{otherwise,}\end{cases} \tag{25}$$

we halved the step length until a significant objective increase is achieved in terms of Armijo rule with coefficient c_1 set to 0.1. We iterated until both the relative change in design variables and the relative change in the objective value dropped below 10^{-6}. The structure of the adopted optimisation strategy is summarised in Algorithm 1.

Algorithm 1 Adopted optimisation strategy.

```
Randomly initialise a_0;  i = 0
while ‖a_i − a_{i−1}‖ ∧ ‖O(a_i) − O(a_{i−1})‖ > 10^{−6}
  compute ∇O(a_i)
  ∇̂O(a_i) = modify ∇O(a_i)
  compute ν̃
  ν = min(ν̃)
  repeat
    a_new = a + ν ∇̂O(a_i)
    ν = ν/2
  until O(a_i + ν∇̂O) ≥ O(a_i) + c_1 ν ∇̂O(a_i)^T ∇̂O(a_i)
  i = i + 1
  a_i = a_new
end
```

3. Results

We demonstrate the proposed objective formulation with two optimisation problems: unimodal and pentamodal metamaterials. As stated in the previous section, both optimisation problems share the same formulation but differ in the definition of the objective function; recall Eqs. (12) and (13). In addition, we show the results for two ground structures depicted in Figure 1, with the larger ground structure being a periodic extension of the smaller one. In all cases, we assumed Young's modulus of elasticity $E = 1$. Since the response of the metamaterial model is linear in E, the homogenised stiffness matrices can be understood as normalised with respect to E.

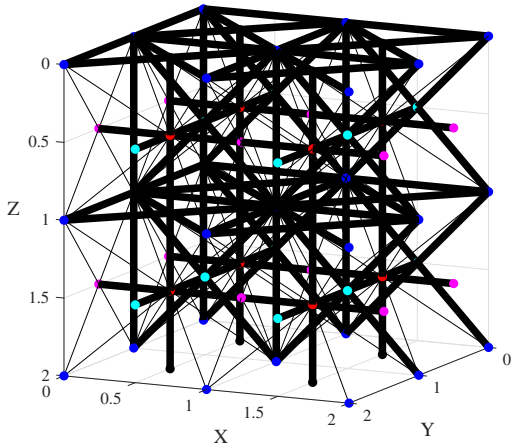

Figure 2. Optimised larger PUC of a unimodal metamaterial with minimised shear modulus in the yz direction.

3.1. Unimodal metamaterial

We start with optimising the microstructure of a unimodal metamaterial with vanishing shear modulus in the yz direction. To this end, we set

$$\mathsf{p} = \begin{bmatrix}0 & 0 & 0 & 1 & 0 & 0\end{bmatrix}^{\mathsf{T}}$$

in the objective definition (12).

Since the whole problem is non-convex, the gradient method renders only local optima. Consequently, the optimised microstructure depends on the initial distribution of cross-sectional areas. The best results obtained out of 100 independent starting points a_0 are shown in Figure 2 for both ground structures, with the line thicknesses indicating the size of the cross-sectional areas.

The homogenised matrix $\mathsf{D}^{\mathrm{hom}}(\mathsf{a}_{\mathrm{opt}})$ of both optimised structures took the form

$$\mathsf{D}^{\mathrm{hom}} = \begin{bmatrix} 6.70 & 1.39 & 1.39 & 0.00 & 0.00 & 0.00\\ 1.39 & 5.32 & 0.00 & 0.00 & 0.00 & 0.00\\ 1.39 & 0.00 & 5.32 & 0.00 & 0.00 & 0.00\\ 0.00 & 0.00 & 0.00 & 0.00 & 0.00 & 0.00\\ 0.00 & 0.00 & 0.00 & 0.00 & 1.39 & 0.00\\ 0.00 & 0.00 & 0.00 & 0.00 & 0.00 & 1.39 \end{bmatrix} \times 10^{-3}\,, \tag{26}$$

and exhibited almost zero value at the position $\mathsf{D}^{\mathrm{hom}}_{4,4}$.

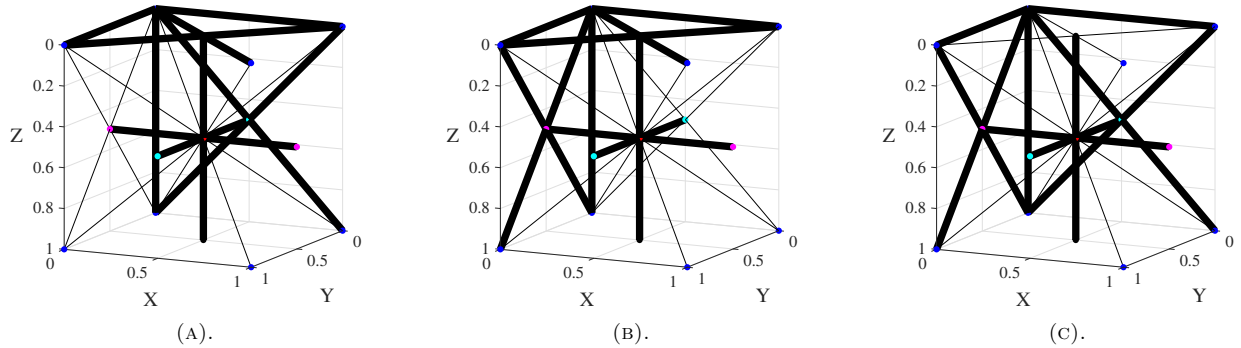

(A). (B). (C).

Figure 3. Optimised PUCs of unimodal metamaterials with minimised shear modulus in yz (A), xz (B) and xy (C) directions.

The value of the associated objective function $\mathcal{O}^{\mathrm{I}}$ was 4.79×10^3.

The best result obtained for the larger ground structure converged to a geometry that is a periodic extension of the best result obtained for the smaller ground structure, i.e. the larger ground structure comprises eight PUCs. Furthermore, we subsequently tested the optimisation of unimodal metamaterial for vanishing shear modules in the xz ($\mathsf{p} = \begin{bmatrix}0 & 0 & 0 & 0 & 1 & 0\end{bmatrix}^{\mathsf{T}}$) and xy ($\mathsf{p} = \begin{bmatrix}0 & 0 & 0 & 0 & 0 & 1\end{bmatrix}^{\mathsf{T}}$) planes. The optimised structures for these scenarios are rotated versions of the metamaterial with a minimised shear modulus in the yz direction, as shown in Figure 3. The corresponding homogenised matrices are – up to a small numerical difference – only permutations of (26). These observations indicate a strong local optimum for such a design, corroborated further by the fact that the same design was achieved for the majority of independent runs with random initial distribution of truss cross-sectional areas.

3.2. Pentamodal metamaterial

As the second example, we optimised the same ground structures for a meta-fluid behaviour, using the objective definition (13) with

$$\mathsf{p} = \begin{bmatrix}\frac{1}{\sqrt{3}} & \frac{1}{\sqrt{3}} & \frac{1}{\sqrt{3}} & 0 & 0 & 0\end{bmatrix}^{\mathsf{T}}.$$

This objective proved to be more challenging than its unimodal counterpart, as there was no strong local optimum. Different optimisation runs with different initial states yielded distinct results with suboptimal performance compared to the existing pentamodal design of Milton and Cherkaev [3], which was attainable with the ground structures we considered.

A common remedy to suppress the sensitivity to local minima widely used in the community of structural optimisation is to use a separable local approximation such as the method of moving asymptotes [30]. Here, we adopt a different strategy that builds on sequential 1D minimisation problems along individual design variables. This approach fits in the provided Algorithm 1 by introducing a gradient modification.

In each iteration, we randomly select a single design variable and compute the modified gradient specifically for that variable. If the modified gradient is non-zero, we perform a 1D line search while maintaining the values of the other design variables constant. If the modified gradient equals zero, we proceed to the subsequent iteration, iterating through the randomly selected design variables until the optimised structure is achieved.

Clearly, such a modification leads to an increase in the number of iterations. Starting with all cross-sectional areas at the lower bound produced a design that corresponded to the known pentamodal design by Milton and Cherkaev [3]. Admittedly, the results remain highly sensitive to the initial conditions. Even with random initialisation of cross-sectional areas from a uniform distribution $[\underline{a}; \frac{\overline{a}}{10}]$, the majority of optimisation cases ended up in the known pentamodal design. We observed that optimisation with smaller values of initial variables tends to result in a higher objective function value than optimisation using larger ones.

The best obtained PUCs of the pentamodal material are shown in Figure 4. Similarly to the unimodal metamaterial, the larger PUC converges towards a geometry composed of eight smaller identical PUCs. For completeness, we list the homogenised matrix $\mathsf{D}^{\mathrm{hom}}$

$$\mathsf{D}^{\mathrm{hom}} = \begin{bmatrix}7.56 & 7.56 & 7.56 & 0.00 & 0.00 & 0.00\\ 7.56 & 7.56 & 7.56 & 0.00 & 0.00 & 0.00\\ 7.56 & 7.56 & 7.56 & 0.00 & 0.00 & 0.00\\ 0.00 & 0.00 & 0.00 & 0.00 & 0.00 & 0.00\\ 0.00 & 0.00 & 0.00 & 0.00 & 0.00 & 0.00\\ 0.00 & 0.00 & 0.00 & 0.00 & 0.00 & 0.00\end{bmatrix} \times 10^{-4}, \quad (27)$$

with objective function achieving a value of 4.27×10^3. Note that the result for the $2 \times 2 \times 2$ ground structure features two interconnected networks and thus its homogenised response is twice as stiff compared to the stiffness of the classical metafluid structure shown in Figure 5.

4. Summary

This contribution dealt with optimising metamaterials for desired unimodal and pentamodal behaviour. The material PUCs were modelled as discrete truss systems, whose effective metamaterial properties were

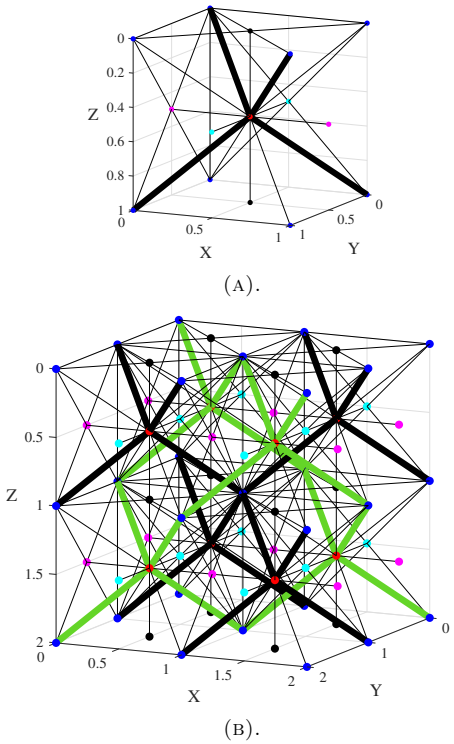

FIGURE 4. Optimised smaller (A) and larger (B) PUCs of a pentamodal metamaterial with maximised bulk modulus. The larger PUC of the pentamodal metamaterial consists of two independent structures (plotted in black and green).

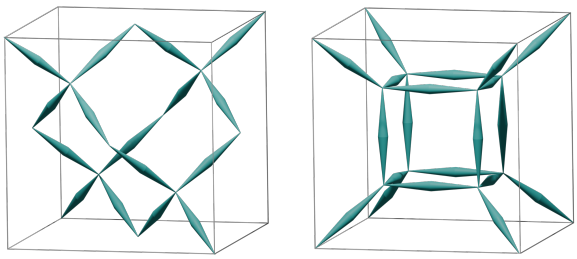

FIGURE 5. Examples of existing pentamodal materials: (left) a microstructure proposed by Milton and Cherkaev [3], and (right) an alternative design by Guo and coworkers [10].

determined using the first-order numerical homogenisation, providing us with a link between their microstructure and macroscopic behaviour to be optimised.

We formulated the objective function on the basis of a projected stiffness and sorted eigenvalues of the homogenised stiffness matrix. The unimodal metamaterials were designed to be significantly more compliant in a chosen shear direction compared to other modes of deformation. The pentamodal metamaterial targeted maximal bulk modulus while diminishing the remaining eigenvalues of the homogenised stiffness matrix.

The optimisation was performed using the steepest ascent method, supplemented with the line search algorithm and constrained by upper and lower bounds for individual cross-sectional areas. To suppress the algorithm's attraction to local minima, we proposed a simple modification of the steepest ascent, which sequentially performs a series of 1D minimisations along individual design variables. In the case of pentamodal material, this modification significantly improved the optimisation results by reducing the number of independent optimisation runs necessary to render a performant solution.

ACKNOWLEDGEMENTS

NŠ and MT acknowledge support by the Czech Science Foundation, Project No. GA22-15524S. MD's work was supported by the Grant Agency of the Czech Technical University in Prague, grant No. SGS24/038/OHK1/1T/11, and co-funded by the European Union under the project ROBOPROX – Robotics and Advanced Industrial Production (reg. no. CZ.02.01.01/00/22_008/0004590).

REFERENCES

[1] E. Barchiesi, M. Spagnuolo, L. Placidi. Mechanical metamaterials: a state of the art. *Mathematics and Mechanics of Solids* **24**(1):212–234, 2019. https://doi.org/10.1177/1081286517735695

[2] O. Sigmund. A new class of extremal composites. *Journal of the Mechanics and Physics of Solids* **48**(2):397–428, 2000. https://doi.org/10.1016/S0022-5096(99)00034-4

[3] G. W. Milton, A. V. Cherkaev. Which elasticity tensors are realizable? *Journal of Engineering Materials and Technology* **117**(4):483–493, 1995. https://doi.org/10.1115/1.2804743

[4] A. Martin, M. Kadic, R. Schittny, et al. Phonon band structures of three-dimensional pentamode metamaterials. *Physical Review B* **86**(15):155116, 2012. Publisher: American Physical Society. https://doi.org/10.1103/PhysRevB.86.155116

[5] A. O. Krushynska, P. Galich, F. Bosia, et al. Hybrid metamaterials combining pentamode lattices and phononic plates. *Applied Physics Letters* **113**(20):201901, 2018. https://doi.org/10.1063/1.5052161

[6] C. W. Cushing, M. J. Kelsten, X. Su, et al. Design and characterization of a three-dimensional anisotropic additively manufactured pentamode material. *The Journal of the Acoustical Society of America* **151**(1):168–179, 2022. https://doi.org/10.1121/10.0009161

[7] C. Gustavo Méndez, J. M. Podestá, O. Lloberas-Valls, et al. Computational material design for acoustic cloaking. *International Journal for Numerical Methods in Engineering* **112**(10):1353–1380, 2017. https://doi.org/10.1002/nme.5560

[8] A. Amendola, G. Carpentieri, L. Feo, F. Fraternali. Bending dominated response of layered mechanical metamaterials alternating pentamode lattices and confinement plates. *Composite Structures* **157**:71–77, 2016. https://doi.org/10.1016/j.compstruct.2016.07.031

[9] P. N. Lymperopoulos, E. E. Theotokoglou. Computational analysis of pentamode metamaterials for antiseismic design. *Procedia Structural Integrity* **26**:263–268, 2020. https://doi.org/10.1016/j.prostr.2020.06.033

[10] D. Guo, S. Jiang, Y. Zhou, et al. Ultrahigh compression-shear ratio of sandwich pentamode metamaterials. *Composite Structures* **322**:117331, 2023. https://doi.org/10.1016/j.compstruct.2023.117331

[11] Y. Huang, X. Lu, G. Liang, Z. Xu. Pentamodal property and acoustic band gaps of pentamode metamaterials with different cross-section shapes. *Physics Letters A* **380**(13):1334–1338, 2016. https://doi.org/10.1016/j.physleta.2016.01.041

[12] M. Kadic, T. Bückmann, R. Schittny, et al. Pentamode metamaterials with independently tailored bulk modulus and mass density. *Physical Review Applied* **2**(5):054007, 2014. https://doi.org/10.1103/PhysRevApplied.2.054007

[13] B. Kumar, A. Banerjee, B. Manna. Effect of finite mass on phononic band structure of face centered pentamodal lattice. *Mechanics Research Communications* **124**:103933, 2022. https://doi.org/10.1016/j.mechrescom.2022.103933

[14] F. Fraternali, A. Amendola. Mechanical modeling of innovative metamaterials alternating pentamode lattices and confinement plates. *Journal of the Mechanics and Physics of Solids* **99**:259–271, 2017. https://doi.org/10.1016/j.jmps.2016.11.010

[15] K. Mohammadi, M. R. Movahhedy, I. Shishkovsky, R. Hedayati. Hybrid anisotropic pentamode mechanical metamaterial produced by additive manufacturing technique. *Applied Physics Letters* **117**(6):061901, 2020. https://doi.org/10.1063/5.0014167

[16] C. Cai, R. Guo, X. Wang, et al. Effect of anisotropy on phononic band structure and figure of merit of pentamode metamaterials. *Journal of Applied Physics* **127**(12):124903, 2020. https://doi.org/10.1063/1.5140610

[17] Y. Huang, X. Zhang, M. Kadic, G. Liang. Stiffer, stronger and centrosymmetrical class of pentamodal mechanical metamaterials. *Materials* **12**(21):3470, 2019. https://doi.org/10.3390/ma12213470

[18] O. Sigmund. Materials with prescribed constitutive parameters: An inverse homogenization problem. *International Journal of Solids and Structures* **31**(17):2313–2329, 1994. https://doi.org/10.1016/0020-7683(94)90154-6

[19] D. Zhang, X. Zhai, L. Liu, X.-M. Fu. An optimized, easy-to-use, open-source GPU solver for large-scale inverse homogenization problems. *Structural and Multidisciplinary Optimization* **66**(9):207, 2023. https://doi.org/10.1007/s00158-023-03657-y

[20] P. Vogiatzis, S. Chen, X. Wang, et al. Topology optimization of multi-material negative Poisson's ratio metamaterials using a reconciled level set method. *Computer-Aided Design* **83**:15–32, 2017. https://doi.org/10.1016/j.cad.2016.09.009

[21] S. Watts, D. A. Tortorelli. A geometric projection method for designing three-dimensional open lattices with inverse homogenization. *International Journal for Numerical Methods in Engineering* **112**(11):1564–1588, 2017. https://doi.org/10.1002/nme.5569

[22] F. Wang, O. Sigmund, J. Jensen. Design of materials with prescribed nonlinear properties. *Journal of the Mechanics and Physics of Solids* **69**:156–174, 2014. https://doi.org/10.1016/j.jmps.2014.05.003

[23] H.-W. Dong, S.-D. Zhao, X.-B. Miao, et al. Customized broadband pentamode metamaterials by topology optimization. *Journal of the Mechanics and Physics of Solids* **152**:104407, 2021. https://doi.org/10.1016/j.jmps.2021.104407

[24] Z. Li, Z. Luo, L.-C. Zhang, C.-H. Wang. Topological design of pentamode lattice metamaterials using a ground structure method. *Materials & Design* **202**:109523, 2021. https://doi.org/10.1016/j.matdes.2021.109523

[25] Z. Zou, F. Xu, Y. Pan, T. Fang. Bandgap properties and multi-objective optimization of double-cone pentamode metamaterials with curved side. *Physica Scripta* **98**(3):035833, 2023. https://doi.org/10.1088/1402-4896/acb5cc

[26] J. C. Michel, H. Moulinec, P. Suquet. Effective properties of composite materials with periodic microstructure: a computational approach. *Computer Methods in Applied Mechanics and Engineering* **172**(1-4):109–143, 1999. https://doi.org/10.1016/S0045-7825(98)00227-8

[27] M. Doškář, J. Novák. A jigsaw puzzle framework for homogenization of high porosity foams. *Computers & Structures* **166**:33–41, 2016. https://doi.org/10.1016/j.compstruc.2016.01.003

[28] N. Jošková, M. Doškář. Effect of geometry on homogenised properties of selected auxetic metamaterials. *Acta Polytechnica CTU Proceedings* **49**:20–25, 2024. https://doi.org/10.14311/APP.2024.49.0020

[29] J. Nocedal, S. J. Wright. *Numerical optimization.* Springer series in operations research. Springer, New York, 2nd edn., 2006.

[30] K. Svanberg. The method of moving asymptotes – a new method for structural optimization. *International Journal for Numerical Methods in Engineering* **24**(2):359–373, 1987. https://doi.org/10.1002/nme.1620240207